

NATIONAL INSTITUTE FOR FUSION SCIENCE

Multifractal Characterization of L- and H-mode
Plasma Edge Turbulence

Milan Rajković and Miloš Škorić

(Received - June 29, 2006)

NIFS-833

June 2006

RESEARCH REPORT
NIFS Series

This report was prepared as a preprint of work performed as a collaboration research of the National Institute for Fusion Science (NIFS) of Japan. The views presented here are solely those of the authors. This document is intended for information only and may be published in a journal after some rearrangement of its contents in the future.

Inquiries about copyright should be addressed to the Research Information Office, National Institute for Fusion Science, Oroshi-cho, Toki-shi, Gifu-ken 509-5292 Japan.

E-mail: bunken@nifs.ac.jp

<Notice about photocopying>

In order to photocopy any work from this publication, you or your organization must obtain permission from the following organization which has been delegated for copyright for clearance by the copyright owner of this publication.

Except in the USA

Japan Academic Association for Copyright Clearance (JAACC)
6-41 Akasaka 9-chome, Minato-ku, Tokyo 107-0052 Japan
Phone: 81-3-3475-5618 FAX: 81-3-3475-5619 E-mail: jaacc@mtd.biglobe.ne.jp

In the USA

Copyright Clearance Center, Inc.
222 Rosewood Drive, Danvers, MA 01923 USA
Phone: 1-978-750-8400 FAX: 1-978-646-8600

Multifractal characterization of L- and H-mode plasma edge turbulence

Milan Rajković

Institute of Nuclear Sciences Vinča, Belgrade, Serbia

Miloš Škorić

National Institute of Fusion Science, Toki, Gifu, Japan

Abstract

Measurements of the edge plasma turbulence obtained by reciprocating Langmuir probe are analyzed and tested for self-similarity, long-range dependence and multifractality. We present evidence for the multifractal character existing in both L- and H- mode data and also provide strong support for the local self-similarity in the case of L-mode. However, we show that neither L-mode nor H-mode measurements show self-similarity in the global sense. Moreover, we use several fractal and multifractal measures in addition to some non-standard statistical techniques in order to characterize the L and H-mode fluctuations.

Keywords: plasma, turbulence, intermittency, tokamak, multifractal, long - range dependence, wavelets.

1. Introduction

Edge turbulence measurements represent an important object of current research efforts in understanding plasma confinement in magnetic fusion devices and studies related to this issue focus among other things, on quantification of intermittent aspects of the dynamics (e.g. [1]). Study of turbulence data makes the important contributions to the study of plasma confinement in spherical, as well as, in toroidal devices. Recently, a study devoted to the analysis of self-similar aspect of the turbulence in the MAST device reported results based on the rescaled range analysis and its ability to distinguish between low and high operating regimes (L- and H-mode) with respect to the existence (or lack of) long-range dependence [2]. In particular, this analysis concentrated on detecting long-range behavior in low and high confinement regimes. In recent years several works were reported

addressing the same aspect of confined plasma turbulence in relation to the possible self-organized criticality (SOC) (see e.g. [3], [4], [5]). An important aspect of the long-range dependence (LRD) property is its relationship to the convective aspect of the dynamics since it is assumed that the avalanche-type transport induces LRD. Hence, detection of LRD property is important for understanding the intermittent convective transport, particularly in the scrape-off layer of magnetically confined plasmas. Most (if not all) of these research efforts assume that the processes representing turbulent plasma behavior are self-similar, in the sense that only one scaling parameter is sufficient to describe the self-similar properties of the dynamics. The purpose of this report is to offer clear evidence that turbulent processes taking place during the low and high confinement regimes in the MAST device are multifractal, in the sense that many parameters are needed in order to adequately (and mathematically correctly) characterize the self-similar property. Moreover, we introduce several methods for quantifying multifractal behavior which offer new insights into the properties of turbulence of L and H modes. Several methods for the analysis of turbulent plasma regimes used previously by the present authors may also yield some important information about the underlying dynamics, however they are not well suited for the analysis of multifractal processes [6], [7].

The report is organized in the following manner. Following a brief description of datasets, an overview of long-range dependent processes is given along with the results obtained for the MAST datasets. An important feature of this section is the statistical test of constancy in time of the scaling exponents. Section 4 gives a short overview of multifractal processes and its relationship with the wavelet transform. Results pertaining to this section contain discussion of multifractal properties of the L and H-mode turbulence in the MAST device. Section 5 discusses effects of coupling long-range dependence with intermittency and the possibility of simultaneous determination of the strength of each of these processes. Concluding remarks are presented in section 6 along with the suggestions for future research activities.

2. MAST edge turbulence datasets

Three datasets are analyzed in this report, obtained by courtesy of R. O. Dandy (EU-RATOM/UKAEA Fusion Association, Culham Science Center, U.K.) and B.D. Dudson (Dept. of Physics, University of Oxford, U. K.). These datasets consist of ion saturation current (I_{sat}) measurements obtained by a moveable Langmuir probe positioned at the outboard midplane on MAST device[2]. The advantage of studying ion saturation current lies in the fact that it carries information about bursts that carry large amounts of particles. Sampling frequency was 1MHz. The datasets were taken during two confinement regimes: L-mode and a dithering H-mode. The L-mode is represented by two datasets labeled 6861 (high density L-mode) and 9035. Dataset 9031 is a dithering H-mode with heating power close to a threshold for L-H transition with intermittent high frequency

edge localized modes. These signals are represented in Fig. 1. Further details pertaining to the datasets may be found in [2].

3. Quantification of long-range dependence

Widely used methods for characterization of plasma turbulence include probability distribution function (PDF), autocorrelation function (ACF) and power spectrum, while recently several papers address the topic of possible long-range dependence in the edge turbulence of toroidal magnetic confinement devices. Upon getting a Hurst exponent in the range $0.5 < H < 1$, the authors often make conclusions concerning the global self-similar properties of such signals, particularly in relationship with the Self-Organized criticality (SOC) models. (e.g. [1]). However, self-similarity is a strong statistical property which intuitively may be defined as a property of scale invariance. This property implies that all scales have equal importance and hence, there is no characteristic scale controlling the dynamics. The notion of self-similar process is defined as follows.

Definition 1. A random process $X(t), t > 0$ is called self-similar if for any $a > 0$, there exists $b > 0$, such that

$$X(at) \stackrel{\circ}{=} bX(t).$$

and the following property may be proved.

Theorem 2. (Lamperti). If random process $X(t), t \geq 0$ is nontrivial, stochastically continuous at 0, and self-similar, then there exists unique $H \geq 0$ such that $b = a^H$. If $X(0) = 0$, then $H > 0$. A self-similar process with parameter H is usually denoted as H -ss.

Such a process, evidently, cannot be stationary. Long-range dependence, on the other hand, is associated with *stationary processes* and may be defined through spectral density. The stationarity issue may be avoided if, for example, linear filtering is used which produces stationary process. In such a case one may define a quasi spectral density as a function of spectral density of filtered stationary process and transfer function of the filter. An example is the spectrum of the fractional Brownian motion.

A stationary process $X(t)$ is called long-range dependent (LRD) process if its autocorrelation function or spectral density behave as

$$r(k) \sim c_r k^{\alpha-1} \quad \text{as } k \rightarrow \infty, \quad \alpha \in (0, 1). \quad (1)$$

or

$$\Gamma_X(\nu) \sim c_f |\nu|^{-\alpha} \quad \text{as } \nu \rightarrow 0, \quad \alpha \in (0, 1). \quad (2)$$

Equations (1) and (2) imply that the covariances $r(k)$ decay so slowly, that

$$\sum_{k=-\infty}^{\infty} r(k) = \infty, \quad \text{or equivalently } \Gamma_X(0) = \infty.$$

There is a close relationship between long-range dependence and self-similar process as increments of any finite variance H - *sssi* process (*sssi* stands for self-similar stationary increments) have LRD, as long as $1/2 < H < 1$, with H and α related through

$$\alpha = 2H - 1.$$

The self-similarity exponent H is usually called the Hurst exponent. However, a Hurst exponent $H > 1/2$ does not necessarily imply long time correlations like those found in fractional Brownian motion. For example, Markov processes which by construction have no memory, may also exhibit long-time correlations [8]. The statement that $H > 1/2$ (persistence), or $H < 1/2$ (antipersistence) imply that correlations may be deduced from a simple argument [9]. Calculating the autocorrelation as:

$$2 \langle \Delta x(t - \Delta t) \Delta x(t + \Delta t) \rangle = \langle (\Delta x(t - \Delta t) + \Delta x(t + \Delta t))^2 \rangle - \langle \Delta x^2(t - \Delta t) \rangle - \langle \Delta x^2(t + \Delta t) \rangle,$$

where $\Delta x(t + \Delta t) = x(t + \Delta t) - x(t)$ and $\Delta x(t - \Delta t) = x(t) - x(t - \Delta t)$. If the process, which is assumed to be stochastic, has *stationary increments*, requiring that the mean square fluctuation from any $x(t)$ scales as [10]

$$\langle (\Delta x(t + \Delta t) - x(t))^2 \rangle = c \Delta t^{2H}.$$

Since the scaling relationship depends only on Δt and not on t , rescaling the autocorrelation function by the mean square fluctuation

$$C(-\Delta t, \Delta t) = \frac{\langle \Delta x(t - \Delta t) \Delta x(t + \Delta t) \rangle}{\langle \Delta x^2(\Delta t) \rangle},$$

the following relationship is obtained:

$$C(-\Delta t, \Delta t) = 2^\alpha - 1 = 2^{2H-1} - 1. \quad (3)$$

Hence any $H \neq 1/2$ implies autocorrelations. The crucial part of the above derivation is that the autocorrelations may exist for $H \neq 1/2$ only if the increments are stationary. Hence an empirical measurement (or theoretical prediction) of Hurst exponent, without evidence for stationarity of increments (or explicit evidence that the process possesses memory) cannot be accepted as evidence for autocorrelations in the data. Since the data for both L and H modes do not have stationary increments due to the extreme increment value excursions as evident in Fig. 2, the signals should be carefully inspected for stationarity, for example by dividing the signal into blocks of equal length which are essentially stationary with respect to the first and second moments. It is interesting to notice that compared to the other two signals, signal 6861 has the largest number of segments with stationary

increments, in spite of having the largest bursts. The LRD analysis presented here is based on the discrete wavelet technique of stochastic processes[13], while more details on the importance of the stationarity property may be found in [12]. Details of the wavelet techniques used in the determination of Hurst exponent may be found, for example in [13] and [14], and we mention here only the most important aspects.

3.1. Wavelet transform of scaling processes

Although the wavelet theory was originally developed for the analysis of deterministic finite energy processes, applications to stochastic processes, in particular to turbulence phenomena, have been very successful in recent years. Since the wavelet transform partitions the data into different frequency components and analyzes each component with a resolution matched to its scale, the coefficients may be used to collect microscopic information about the scale-dependent properties of the data. It has been shown that for a H-ss process the wavelet coefficients $d_X(j, k)$ exactly reproduce the self-similarity property of the process. In particular, for sufficiently large scales j , the following relationship holds

$$\log_2 E d_X^2(j, k) \sim j\alpha + C = j(2H - 1) + C, \quad (4)$$

where C is constant independent of location index k and E denotes the expectation value. The above property in the wavelet domain allows the analysis of stationary, short-range dependent (SRD) processes $d_X(j, \cdot)$ for each j . A quantity of central importance is the non-parametric, unbiased variance of the process $d_X(j, \cdot)$

$$\mu_j = \frac{1}{n_j} \sum_{k=1}^{n_j} |d_X(j, k)|^2, \quad (5)$$

where n_j is the number of coefficients at octave j available for the analysis. Based on the power-law expression (4), the scaling exponent α (and hence H) could be simply obtained by inspecting the slope of $\log_2 \mu_j$ vs. j . This scaling behavior is detected by means of the so called log-scale diagrams which display $\log \mu_j$ as a function of scale j . Confidence intervals about the $\log \mu_j$ increase monotonically with j as larger and larger scales are encountered and region of alignment in the log-scale diagram is detected where up to statistical variation, the $\log_2 \mu_j$ values fall on a straight line. Since possible LRD processes are analyzed, the alignment should be detected for large values of scales j (e.g. ≥ 6). Hence a log-scale diagram may be considered a spectral estimator where large scales correspond to low frequencies.

3.2. Log-scale diagrams of MAST datasets

The log-scale diagrams are presented in Figs. 3, 4 and 5 corresponding to L-mode 6861, H-mode 9031 and L-mode 9035 respectively. According to these diagrams L-mode turbulent

signals 6861 and 9035 display LRD while H-mode is practically white noise with Hurst exponent almost equal to $1/2$, hence not an LRD process. We also estimate coefficients c_f which take positive real values. Their importance lies in the property of long-range dependence that the sum over all correlations is large (actually infinite), but individually their sizes (which can be arbitrarily small) at large lag is controlled by c_f . Moreover, confidence intervals around mean estimates of LRD are proportional to the square root of c_f . In Table 1 we present LRD parameter estimates for all three signals, along with the confidence intervals

	L-mode 6861	H-mode 9031	L-mode 9035
α	0.254	0.03	0.264
H	0.627 [0.577 0.676]	0.515 [0.438 0.532]	0.632 [0.587 0.677]
c_f	0.1225 [0.0719 0.1956]	0.1775 [0.058 0.4187]	0.03 [0.023 0.120]

Table 1: Global indicators of self-similar character of the three signals. Confidence intervals are presented in square brackets.

We have also performed the LRD parameter evaluation using the Allan variance and the obtained H values correspond well with the above values, being 0.620, 0.52 and 0.61 for signals 6861, 9031 and 9035 respectively. Characteristic feature of all log-scale diagrams obtained here is the large variability in top portion of the spectrum (large scales, usually greater or equal to 6), which suggests that particular care should be taken in interpreting the (possible) global Hurst exponent[14], requiring careful examination of the stationarity properties of each signal and possible evaluation of local Hurst exponents.

3.3. Testing time constancy of scaling exponents

Large variability in the scaling process of the log-scale diagram may easily yield erroneous detection of scaling regions when actually the data is not scaling but is non-stationary (in a non-scaling sense). Hence any conclusion relating to the estimation of the global Hurst exponent (for the entire time series) calls for detecting constancy (or non constancy) of the scaling exponent. The test consists in dividing the data set into non-overlapping blocks and estimation of scaling exponent for each of them[15]. The wavelet based estimates may be assumed as uncorrelated Gaussian variables with unknown means but known variances. The null hypothesis is that exponents for each block are equal, although unknown, and the test is so devised that if the null-hypothesis is rejected one may conclude that the data is *both non-scaling and non-stationary*. The size of each block must be chosen in such a way so that the scaling region may be measurable over a sufficiently wide range of scales. Consequently, the number and size of the blocks should be large enough to see or follow precisely enough the variation in time of exponent H . For L-modes 6861 and 9035 we obtained very good constancy of exponent H for several sets of block sizes (between 5

and 30) and several scaling regions, as shown in Figs 6 and 7. Hence the null hypothesis was accepted in this case. In contrast to this, the null hypothesis was rejected in case of an H-mode dataset 9031 for some of the dataset partitioning as shown in Fig 8, for the case of partitioning into 10 blocks. However, for the case of 5 blocks (small number of blocks) the null hypothesis is accepted due to the fact that the blocks are too wide to reveal the variation in H . The null-hypothesis is again rejected for small block sizes (≥ 20) because the statistical fluctuations of the estimates are large enough to mask the temporal variation of exponents H . Therefore, our final decision was to reject the hypothesis of constancy of exponent H over blocks. An important feature of the log-scale diagrams for each block (as well as for the entire signal) is that for large scales the $\log_2 \mu_j$ practically does not change as a function of scale j (the slope is practically equal to 0 within the confidence interval). But in order to deduce long-range dependence the scaling at large scales is absolutely necessary, so rejection of the null hypothesis is more a consequence of the non-scaling than the scaling variability. Based on these considerations we conclude that the long-range dependence is not present in this dataset. The non-stationarity (in the non-scaling sense) and inability to obtain the common scaling regions for the median number of blocks (10 in this case) for the H-mode dataset 9031 is probably due to the H-mode plasma being in the threshold region of the low to high confinement transition. This transition state and its influence on intermittency properties may be responsible for the high variability of the Hurst exponent.

3.4. Randomization method in detecting long range correlations

The basic idea of a randomization method is to decouple the short-range from the long-range correlations in order to more clearly inspect the effects of the long-range dependence. Following partitioning of the time series into a number of blocks of equal size, three types of randomization procedures are performed. The first one is the external randomization where the content of each block remains intact while the order of the block is randomly shuffled. If the series is sufficiently long, the autocorrelations should exhibit significant correlations beyond the block size. The next procedure is internal randomization, where the order of the blocks remains the same while the contents of each block are randomized. In this case if the dataset has long memory the autocorrelation function following such a procedure will still exhibit power-law behavior. Finally, there is a two level randomization where each block is further subdivided into smaller blocks and the randomization procedure is performed for the contents of each block as well as the order of the larger blocks is shuffled. As a result of this procedure, both short and long range correlations (across multiple blocks) are preserved, while medium range correlations (across multiple smaller blocks within the same block) are equalized. In our tests the block size was set at 20 and the results are presented in Figs 9, 10 and 11. External randomizations for all signals causes elimination of all correlations beyond the block size. Internal randomization

preserves power law behavior for the case of L-mode signals 6861 and 9035, however this is not so clear for the case of H-mode 9035 which is almost exponential. Also two-level randomization distorts the medium-range correlations in the case of L-modes 6861 and 9035, while this is not the case for H-mode signal 9035.

Finally, we may conclude that the L-modes 6861 and 9035 definitely display long-range correlations, while the H-mode signal shows white noise like properties and the lack of long-range dependence due to the non-stationarity and lack of constancy of the H exponent over time. In addition, we argue that the relationship of the power-law behavior at small frequencies with high variability of the block-data Hurst exponents at large scales (small frequencies) suggests that strong intermittent bursts at small scales (high frequencies) have a large impact on the dynamics at large scales. Hence, a simultaneous evaluation of the effects of long-range dependent effects and intermittency could give some more insight into this phenomenon.

4. Multifractal properties of datasets

4.1. Basic properties of multifractal processes

Definition 3. A random process $X(t)$, $t > 0$ is called Multifractal process (mf), if for any $a > 0$, there exists a random function $M(a)$ such that

$$X(at) \stackrel{\circ}{=} M(a)X(t).$$

Here the scaling (self-similar) factor $M(a)$ is a random variable, whose distribution does not depend on the particular time instant t . Exact self-similar process is a degenerate example of a multifractal, with $M(a) = ah$ and sometimes is referred to as a mono-fractal process. The generalized self-similarity index is defined as $h(a) = \log_a M(a)$. Therefore the above relationship may be rewritten as

$$X(at) \stackrel{\circ}{=} a^{h(a)}X(t). \quad (6)$$

In contrast to self-similar processes, the index $h(a)$ is a random function of a . The exponent $h(a)$ is referred to as the Hölder exponent.

Definition 4. A random process $X(t)$, $t > 0$ is called Multifractal process if it has stationary increments and satisfies

$$E(|X(t)|^q) = C(q)^{\tau(q)+1}, \quad \text{for all } t \in T; q \in Q,$$

where T and Q are intervals on the real line, $\tau(q)$ and $C(q)$ are functions with domain Q . Moreover, we assume that T and Q have positive lengths, and that $0 \in t, [01] \subseteq q$.

Function $\tau(q)$ is the scaling function of a multifractal process. All $\tau(q)$ has the intercept -1 , which is implied by $E(|X(t)|^q) = 0$ at $q = 0$. As a special case, monofractal has the linear scaling function $\tau(q) = Hq - 1$. It is also shown that $\tau(q)$ is always a concave function for all multifractal functions.

Based on the expression for the self-similar process (strict sense),

$$X(at) \stackrel{\circ}{=} a^H X(t) \quad (7)$$

one may question whether this relationship holds for the datasets under study and consequently question into the meaning of the determined Hurst exponent in the analysis of the long-range dependence. As an initial step in this direction our aim here is to determine whether the above expression is valid for the L and H mode datasets of the MAST confinement regimes.

Local exponents $h(a)$ are evaluated through the modulus of the maxima values of the wavelet transform at each point in the time series. Then, the scaling partition function $Z(q)$ is defined as the sum of the q -th powers of the local maxima of the modulus of the wavelet transform coefficients at scale a . For small scales, the following relationship is expected

$$Z(q) \sim a^{\tau(q)}. \quad (8)$$

For certain values of q , the exponents $\tau(q)$ have familiar meanings. In particular $\tau(2)$ is related to the scaling exponent of the power spectra, $\Gamma(\nu) \sim 1/\nu^\beta$, as $\beta = 2 - \tau(2)$. For positive q , $Z(q)$ reflects the scaling of the large fluctuations and strong singularities, while for negative q , $Z(q)$ reflects the scaling of the small fluctuations and weak singularities [11]. Hence, the scaling exponent $\tau(q)$ may reveal much about the underlying dynamics. Monofractal signals display linear $\tau(q)$ spectrum,

$$\tau(q) = qH - 1, \quad (9)$$

where H is the global Hurst exponent. For multifractal signals $\tau(q)$ is a nonlinear function $\tau(q) = qh(q) - D(h)$, where

$$h(q) \equiv d\tau(q)/dq \quad (10)$$

is non-constant Hölder exponent (local Hurst exponent). and $D(h)$ is the fractal dimension

$$D(h) = qh - \tau(q). \quad (11)$$

This function, also known as the Legendre multifractal spectrum since it is obtained by taking the Legendre transform of $\tau(q)$, is very useful to characterize multifractals. It is smooth and continuous and shows a single maximum. It is also universal in the sense that the same general type of function characterizes many different types of multifractal phenomena, or that an identical function characterizes a whole range of phenomena. The maximum value of $D(h)$ is the capacity dimension D_0 of the multifractal support, hence

it may be an integer. The $D(h) = h$ line is tangent to the $D(h)$ vs. h plot, and the point of contact gives the information dimension D_1 . The other generalized dimensions are arranged around the $D(h)$ vs. h curve, positive values to the left of the maximum, and negative values to the right. The spread of the $D(h)$ vs. h curve is a measure of clustering of the data. Large positive $D(h)$ (low h values) correspond to points having small higher moments, so that large data values (or concentrations of data points) are clustered around these points. Large negative $D(h)$ (high h values) correspond to points with higher moments, so that low data values (or low concentrations of data points) are found close to these points. In a typical multifractal, there is a strong clustering of the data, whereas in a monofractal the $D(h)$ vs. h plot would be a single spike (all generalized dimensions are equal to D_0) indicating that clustering is no more than would be expected from the simple generating mechanism, or from a random process. The curve $D(h)$ vs. h is not necessarily symmetric. Most commonly the left side is steeper than the right one. This indicates that dense clusters, or clusters of exceptional large values, are rare relative to sparse concentrations, or low values.

4.2. Multiscale diagrams and wavelet coefficients

In the wavelet transform formalism, the partition function is defined as

$$Z(q) = \lim_{j \rightarrow -\infty} \log E |d_X(j, k)|^q.$$

The log-scale diagrams used to inspect the scaling of the variance of the wavelet coefficients, eq.(5), may be generalized to the study of higher order statistics so that the generalized eq.(5) takes the form

$$\mu_j = \frac{1}{n_j} \sum_{k=1}^{n_j} |d_X(j, k)|^q.$$

This expression may be related to the definition 4 of the multifractal process in the following manner. From the definition of self-similarity, the moments of the random process $X(t)$ satisfy

$$E(|X(t)|^q) = E(|X(1)|^q) \cdot |t|^{qH}, \quad \forall t.$$

The property of wavelet coefficients

$$E|d_X(j, k)|^q = E|d_X(0, k)|^q \cdot 2^{j(\tau(q)+q/2)},$$

implies that

$$E\mu_j^q = C(q)2^{j(\tau(q)+q/2)}, \quad \forall j,$$

with

$$\tau(q) = qH.$$

This relationship indicates that self-similarity (and multifractality) may be inferred by testing the linearity of $\zeta(q)$ with q . For multifractal processes

$$\int |T_X(a, t)|^q dt \approx a^{(\tau(q)+q/2)} \quad (a \rightarrow 0),$$

where $T_X(a, t)$ are continuous wavelet coefficients

$$T_X(a, t) = \langle X | \psi_{a,t} \rangle, \quad a \in R^+, \quad t \in R,$$

and where $\psi_{a,t}$ are dilatations and translations of the mother wavelet ψ_0 . From these expressions $\tau(q)$ may be measured and the Legendre multifractal spectrum may be obtained. Naturally, one is first interested whether $\tau(q)$ takes a simple form $\tau(q) = qH$. For example, self-similar processes, for which

$$\mu_j^q \approx 2^{j(\tau(q)+q/2)},$$

for all scales satisfy $\tau(q) = qH$, and are therefore fractal processes with $h = H$. The multiscale diagram is obtained by plotting $\tau(q) = hq - (1/2)(q-1)$ against q , (together with confidence intervals about $\tau(q)$). If there is no alignment, i.e. the relationship $\tau(q) = qH$ does not hold, a multifractal scaling is deduced. Using the same wavelet formalism we may obtain the $\tau(q)$ vs. q and the Legendre spectrum ($D(h)$ vs. h), and as discussed above they may be used to qualitatively and quantitatively describe the multifractal properties of the signals.

4.3. Multiscale diagrams and multifractal spectra for the L and H modes

Test for multifractal property of the signals are presented in Figs. 12, 13 and 14¹. Diagrams on the left side of each figure show scaling of $\tau(q)$ with q , while diagrams on the right show q -dependence of $h_q (= \tau(q)/q)$. Diagrams clearly illustrate that all three confinement regimes (6861 L-mode, 9031 H-mode and 9035 L-mode) are multifractal processes, and hence cannot be characterized by a single Hurst exponent. Specifically, none of the diagrams on the right (Linear multiscale diagrams) have approximately constant $h(q)$ for positive q (a sign of global scaling). In order to compare this with the monofractal process, in Fig. 15 we show the same diagrams for the *fractal Gaussian noise* where a flat region for positive q is a clear indication of global self similarity. Hence signals of both the low and high confinement regimes are *multifractal processes*. In order to quantify the multifractal properties we present in Figs 16, 17 and 18 the $\tau(q)$ spectra and the corresponding singularity spectra. The singularity spectra (or the Legendre spectra) are obtained from the scaling exponents $\tau(q)$ of the partition function by means of the Legendre transformation. Essentially, the singularity spectrum describes the statistical distribution of the singularity exponents by associating with any given exponent the Hausdorff dimension of

¹Matlab routines developed by P. Abry and D. Veitch were used for this purpose.

the set of points which have the same singularity exponent[11]. It is simple to deduce three key attributes of the multifractal spectrum, namely the left slope, mode and the width spread. By the arguments given earlier, one can deduce that the value corresponding to the most frequent singularity is the information dimension D_0 (mode). This quantity represents actually the most sensitive indicator of the mentioned three geometrical attributes of the multifractal spectrum. Information dimension for the L-mode signal 9035 and the H-mode signal 9031 are very close to 1, however it is somewhat smaller for the L-mode 6861 signal ($D_0 \approx 0.95$). The left side in all three cases is steeper than the right one, indicating that dense clusters, or clusters of exceptional large values are rare relative to spares (low value) concentrations. The mode for the L-mode 6861 is the most positive indicating slightly weaker intermittency compared to other two datasets. Recalling that according to Kolmogorov K41 theory the mode is $1/3$ and since all three signals have modes below this K41 value, the intermittency effects are strong in all three datasets. This suggest that it is important to study the coupling effects of long-range dependence together with intermittency in order to more effectively interpret the dynamics of the two regimes. This issue will be discussed in somewhat more detail later on.

In contrast to the power spectra, which describe the distribution of energy of the signal, the multifractal spectrum describes the distribution of local singularities expressed in terms of the so-called Hölder exponents. Formally, the function X is Hölder continuous with exponent α , $0 < \alpha < 1$, at t_0 if as $|t - t_0| = |\Delta t| \rightarrow 0$,

$$|X(t_0 + \Delta t) - X(t_0)| \leq C |\Delta t|^\alpha.$$

Geometrically, a local singularity at time t_0 can be visualized as a relation between neighborhood fluctuations of a function $X(t)$ and two bounding curves as shown in Fig. 19. To estimate such a singularity, two curves expressed through $X(t_0) \pm C|t - t_0|^\alpha$ may be constructed (where C is a constant). The maximum value of α that locally bounds $X(t)$ in the neighborhood of t_0 between these two curves is the local singularity (bottom-left diagram of Fig. 19). When α is large, the curvatures are narrow thus limiting local fluctuations (bottom-right diagram of Fig. 19). When α is small, two curves have small curvature, thus allowing $X(t)$ to take on large local irregular behavior and when t_0 slides across the time series, the distribution of the resulting α is described by the multifractal spectrum. It has been shown that the local singularity strength can be measured in terms of the wavelet coefficients as[18]

$$h(t) = \lim_{k2^j \rightarrow t} \frac{1}{j} \log_2 |d_X(j, k)|.$$

With the h determined, the multifractal spectrum, sometimes denoted by $f(\alpha)$ because α is used instead of h , measures the distribution of $h(t)$ within a time series and can be also obtained using the standard box-counting technique. The Hölder exponent may be

thus interpreted as a local Hurst exponent, and in the manner that global Hurst exponent carries information about self-similar functions, it characterizes the regularity of a function at a given point of the time-series. A Hölder exponent between 0 and 1 indicates that the signal is continuous but not differentiable at the considered point, and the closer this exponent is to zero, the less regular the function is. Pointwise Hölder exponents, measuring the scaling behavior at infinite resolution, for the two regimes are presented in diagrams of Figs 20, 21 and 22. Hence, all modes are characterized by continuous but not differentiable signals. For comparison purposes, Hölder exponents for the three signals are presented using the large deviation spectra. A large deviation spectrum (LDS) represents coarse grained Hölder exponents which measure scaling behavior at finite resolution. The large deviation spectra which point to discernible differences between the signals for the three confinement regimes are presented in Fig. 23. The x-axis in this diagram represents the Hölder exponents of signals and the y-axis reflects the number of points with the corresponding exponent, i.e. the probability of finding the particular Hölder exponent within the signal. The 6861 L-mode is considerably more regular than the other two, while the 9035 H-mode and 9035 L-mode exhibit surprisingly similar spectra with the L-mode 9035 being slightly more irregular. Recalling the almost stationary increments of the 6861 signal it may be inferred that intermittent burst do not change much the regularity of this signal. Based on these results of the analysis alone, it is clear that all signals are the product of small-scale stochastic plasma turbulence, without large-scale events.

Few words should be devoted to the relationship between the singularity (Legendre) spectrum and the large deviation spectrum. The singularity spectrum represents a concave approximation to the large deviation spectrum (LDS). The LDS yields more robust estimates however at the expense of a loss of information. Hence both spectra should be used in the analysis along with the Hausdorff spectrum which is the most precise spectrum from a mathematical aspect, however very demanding as far as computational time is concerned. The complete analysis of the three spectra will be given elsewhere.

5. Coupled effects of long-range dependence and intermittency

The scaling of the energy spectrum in the high frequency range in all three processes is different from the scaling in the low frequency range. Since the scaling in the low frequency range determines long-range behavior and the scaling in the high frequency range is determined by intermittency effects it is of great importance to study both effects simultaneously on the basis of the model presented in [19] and [20]. Namely it has been argued that the fractional Riesz-Bessel motion (fRB), which represents a Gaussian process which has stationary increments and spectral density of the form

$$\Gamma(\nu) = \frac{c_f}{|\nu|^{2\beta}} \frac{1}{(1 + \nu^2)^\gamma}, \quad (12)$$

with the two fractional parameters satisfying

$$\beta \in (1/2, 3/2) \text{ and } \gamma \geq 0,$$

or

$$\Gamma(\nu) = \frac{c_f}{|\nu|^{2\beta}} \frac{1}{(1 + \nu^2)^\gamma} \frac{\nu^2}{1 + \nu^2}, \quad (13)$$

with the two fractional parameters being

$$\beta \in (1/2, 3/2) \quad \text{and} \quad \beta + \gamma \geq 1/2,$$

may be appropriate to model combined effects of long-range dependence and intermittency. Synergistic action of these two effects is reflected in the scaling of the energy spectrum. It may be easily noticed that the fractional Brownian Motion (fBM) is the limiting case of the expression (12) as $\gamma \rightarrow 0$ and $H = (2\beta - 1)/2$. The importance of these two expressions (12) and (13) in the analysis of turbulent signals stems from the physical meaning of these expressions. The component $|\nu|^{-2\beta}$ signifies the long-range dependence with fractional parameter $\beta = H + 1/2$, while the component $(1 + \nu^2)^{-\gamma}$ indicates second-order intermittency. Therefore, based on the model of the fractional Riesz-Bessel motion it is possible to study both effects simultaneously by determining the corresponding exponents β and γ . In order to illustrate graphically these two effects we show the periodograms for the three processes under study in Figs. 24, 25 and 26. The periodogram I_N of the signal $X(t)$ represents the power spectrum of the *entire signal* according to the expression

$$I_N(\nu) = \frac{1}{2\pi N} \left| \int_0^N e^{-i\nu t} X(t) dt \right|^2,$$

where $N > 0$ is the upper bound of the interval $[0, N]$, on which each $X(t)$ is observed. Naturally, periodograms of segments of the time series may be averaged together to form the power spectral density. The main advantage of the periodogram with respect to the power spectral density, in this particular case, is the ability to clearly disclose the scaling behavior both in the low and in the high frequency range. The negative slope of power-law behavior in the low-frequency range determines the long-range dependence while the steeper negative slope in the high frequency range determines the intermittency strength. Note that the flat region in the low frequency range for the H-mode signal 9035 suggest possible lack of long-range dependence. Also evident is that the slopes in the high frequency region are different, corresponding to the different intermittency effects in the low and high confinement regimes. An estimation procedure based on the wavelet transform, as suggested in [19] and [20], may be used for determining both fractional exponents simultaneously. Details of this procedure and the obtained results will be given elsewhere.

6. Conclusion

One of the main features of the H-mode signal 9035, pertaining to the lack of long-range dependence, is that it shows large temporal variability in the Hurst exponents values evaluated over signal partitioned into equal segments. This variability cannot be inferred from the distribution of means and variances corresponding to the blocks, however may be expected from the distribution of increments over time. The fact that this signal has been recorded close to the threshold of the low-to-high confinement regimes is of particular relevance with respect to the issue of exponents variability and suggests further inquiries into the mechanism of the loss of long-range dependence. On the other hand almost stationary segments in the temporal dynamics of the 6861 increments suggest LRD process. The possible LRD in the signals may be anticipated from the slope of the periodogram at small frequencies (large scales). All turbulent signals are multifractal which indicates that they are only locally self-similar and that many Hurst (Hölder) exponents are necessary in order to quantify the self-similar features. Singularity spectra, obtained with the wavelet transform method, yield information about the distribution of singularities and may be used to estimate several types of dimensions. Information dimension, pertaining to the maximum of the singularity spectrum, is slightly lower for the L-mode signal 6861 due to its higher regularity as compared to signals 9031 and 9035. Detailed analysis of the multifractal features requires analysis of the Hausdorff spectrum, large deviation spectrum and the singularity spectrum, and will be presented in another report. Finally, we suggest that fractional Riesz-Bessel motion may be of relevance for explaining the coupling between long-range dependent dynamics and intermittency.

Acknowledgement *We thank R. O. Dandy (EURATOM/UKAEA) for initiating joint work and for helpful discussion on this subject and B.D. Dudson (U. of Oxford.) and G. Antar (UCSD) for providing us with the datasets. The authors wish to express their gratitude for interest and support to A. Komori and H. Yamada, for partial funding and hospitality (M. R.) under ICDBI-scheme to NIFS and for continuing assistance to S. Ishiguro, A. Ito and H. Okumura.*

References

- [1] G. Antar, G. Counsell, Y. Yu, B. Labombard and P. Devynck, Universality of intermittent convective transport in the scrape-off layer of magnetically confined devices, *Phys. Plasmas*, 10 (2003) 419-428.
- [2] B. D. Dudson, R. O. Dandy, A.Kirk, H. Meyer and G. F. Counsell, *Plasma Phys. Control. Fusion* 47 (2005) 885-901.
- [3] B. Ph. van Milligan, B. A. Carreras, et al., Long-range Correlations and Universality in Plasma Edge Turbulence, *Phys. Plasmas*, 5 (1998) 3632.

- [4] G. Wang, G. Antar and P. Devynck, The Hurst exponent and long-time correlation, *Phys. Plasmas* 7 (2000) 1181-1183.
- [5] B. Ph. van Milligan, C. Hidalgo and B. A. Carreras, Comment on "The Hurst exponent and long-time correlation", *Phys. Plasmas* 7 (2000) 5267-5268.
- [6] M. Rajković, Nonextensive entropy as a measure of time series complexity, *Physica A* 340 (2004) 327-333. Preprint: nlin.CD/0404019.
- [7] M.M. Škorić, M.S. Jovanović and M.R. Rajković, Route to Turbulence in Stimulated Raman Backscattering, *Physical Review E*, 53, (1996), 4056 - 4066.
- [8] K. E. Bassler, G. Gunaratne and J. L. MaCauley, Markov processes, Hurst exponents and nonlinear diffusion equations with applications to finance, preprint.
- [9] P. Embrechts and M. Maejima, *Self-Similar Processes*, Princeton University Press, Princeton, 2002.
- [10] Rl L. Stratonovich, *Topics in the Theory of Random Noise*, Gordon & Breach, N.Y, tr. R. A. Silverman, 1963.
- [11] J. F. Muzy, E. Bacry, A. Arneodo, The multifractal formalism revisited with wavelets, *Int. Journal of Bifurcations and Chaos*, 4 (1994) 245 - 302.
- [12] S. Stoev, M. Taqqu, C. Park, and J. S. Marron, On the wavelet spectrum diagnostic for Hurst parameter estimation in the analysis of Internet traffic, 48 (2005) 423-445.
- [13] P. Abry, P. Flandrin, M. Taqqu and D. Veitch, Wavelets for the analysis, estimation and synthesis of scaling data. In *Self-similar Network Traffic and Performance Evaluation*, K. Park and W. Willinger, Eds. Wiley, 2000.
- [14] S. Stoev, M. Taqqu, C. Park, G. Michaelidis and J. S. Marron, LASS: A tool for the local analysis of self-similarity, technical report 2004-7, 2004, Statistical and Applied Mathematical Sciences Institute, Research Triangle Park.
- [15] D. Veitch and P. Abry, A statistical test for the time constancy of scaling exponents, *IEEE Trans. Signal Processing* 49 (2001) 2325-2334.
- [16] E. Bacry, J. F. Muzy and A. Arneodo, Singularity spectrum of fractal signals from wavelet analysis: Exact results, *J. Stat. Phys.*, 70 (1994) 635-674.
- [17] S. Jaffard, Sur la nature multifractal des processus de Lévy, *C. R. Acad. Sci., Paris, Série 1*, t323: (1997) 971-988.

- [18] P. Goncalves, R. H. Riedi and R. G. Baraniuk, Simple statistical analysis of wavelet-based multifractal spectrum estimation, Proceedings of the 32nd Conference on 'Signals, Systems and Computers', Asilomar, 1998.
- [19] V. Anh, J. Angulo and M. Ruiz-Medina, Possible long-range dependence in fractional random fields, *J. Statist. Plann. & Inference*, 80 (1999) 95-110.
- [20] V. V. Anh, N.N. Leonenko, R. McVinish, Models for fractional Riesz-Bessel motion and related processes, *Fractals* 9 (2001) 329-346.

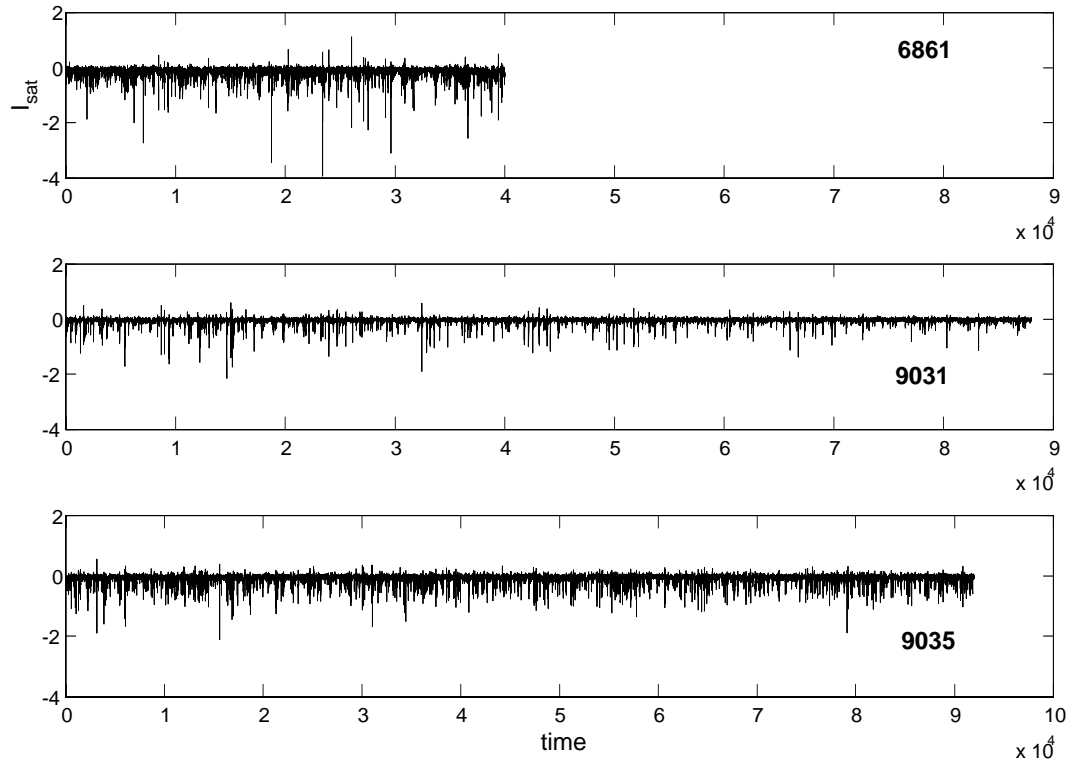


Figure 1: Saturation current as a function of time for the low confinement regime (signals 6861 and 9031) and the high confinement (dithering H-mode) 9035 signal.

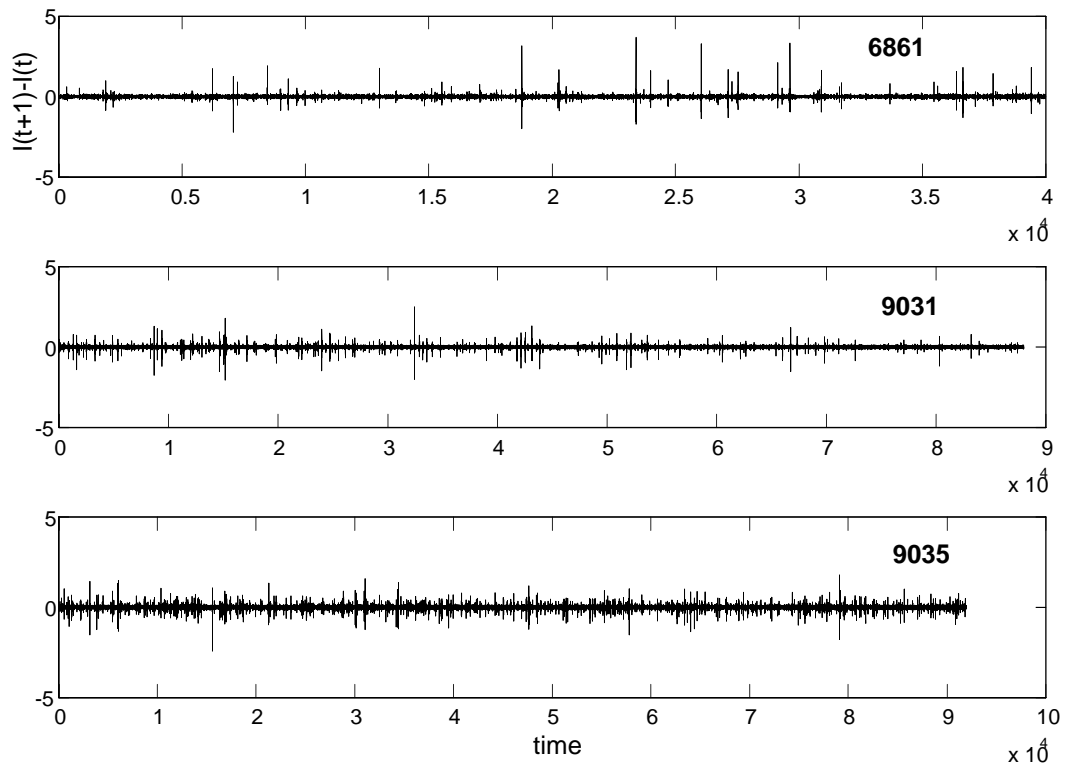


Figure 2: Increment process of the L-mode 6861 and 9035 signals and H-mode signal 9035. Note high excursions in the 6861 signal. In spite of that, this signal also contains more stationary blocks than the other two signals.

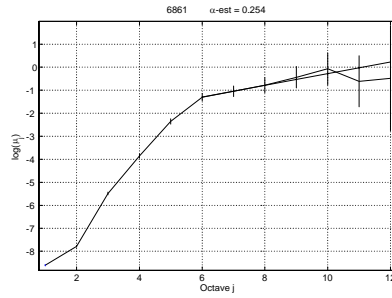


Figure 3: Log-scale diagram displaying scaling of the variance of wavelet coefficients across scales for the L-mode 6861 signal.

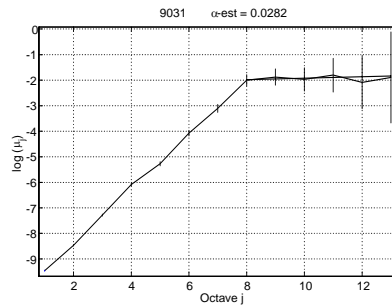


Figure 4: Log-scale diagram for the H-mode 9031 signal. Note the zero slope for high scales indicating lack of long-range dependence.

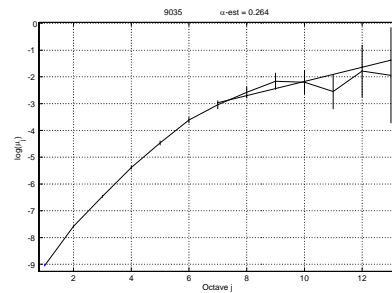


Figure 5: Log-scale diagram displaying scaling of the variance of wavelet coefficients across scales for the L-mode 9035 signal.

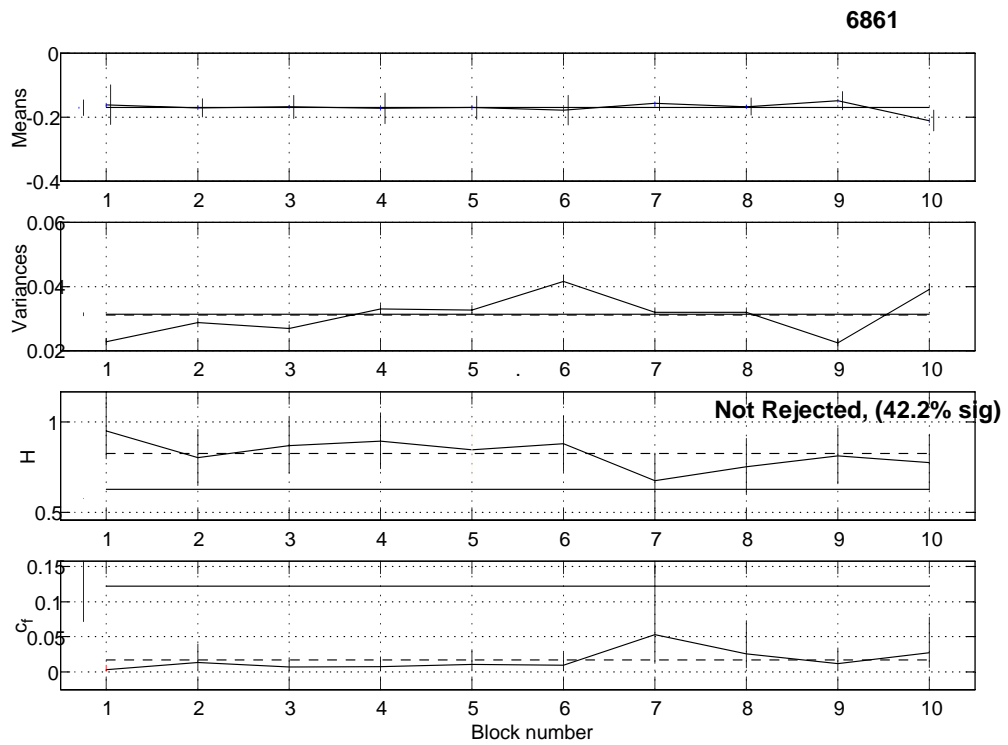


Figure 6: From top to bottom: means, variances, Hurst exponents and c_f 's evaluated over each block for signal 6861. On means and variances diagram horizontal line gives the overall value for the entire series. On H and c_f diagram solid horizontal line indicates the overall value and the dashed line gives the average value.

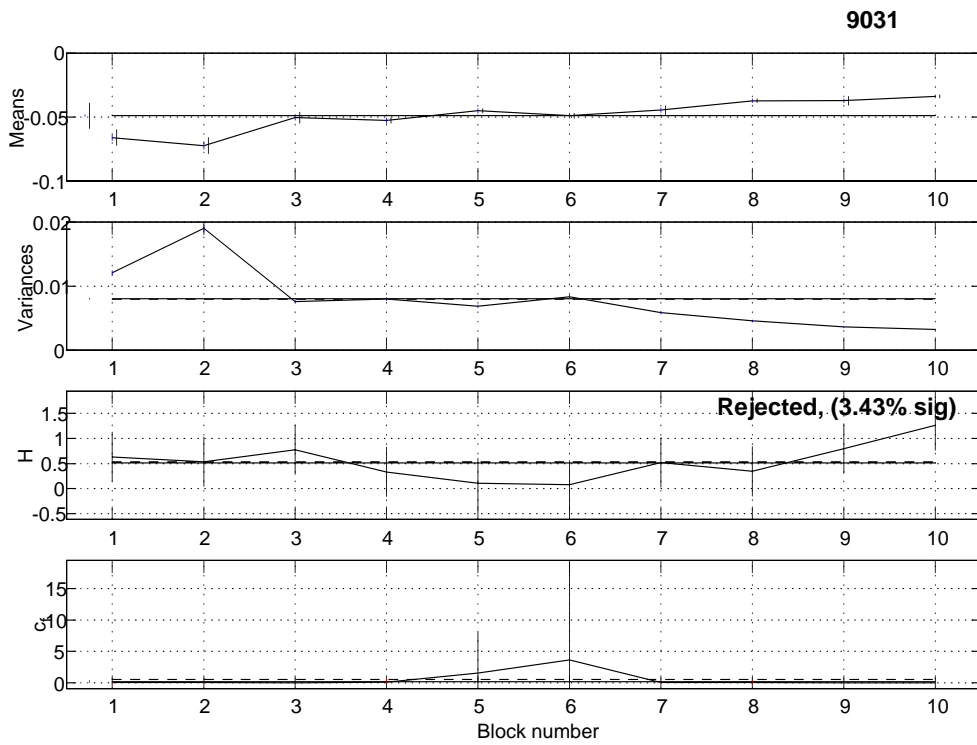


Figure 7: From top to bottom: means, variances, Hurst exponents and c_f 's evaluated over each block for signal 9031. On means and variances diagram horizontal line gives the overall value for the entire series. On H and c_f diagram solid horizontal line indicates the overall value and the dashed line gives the average value.

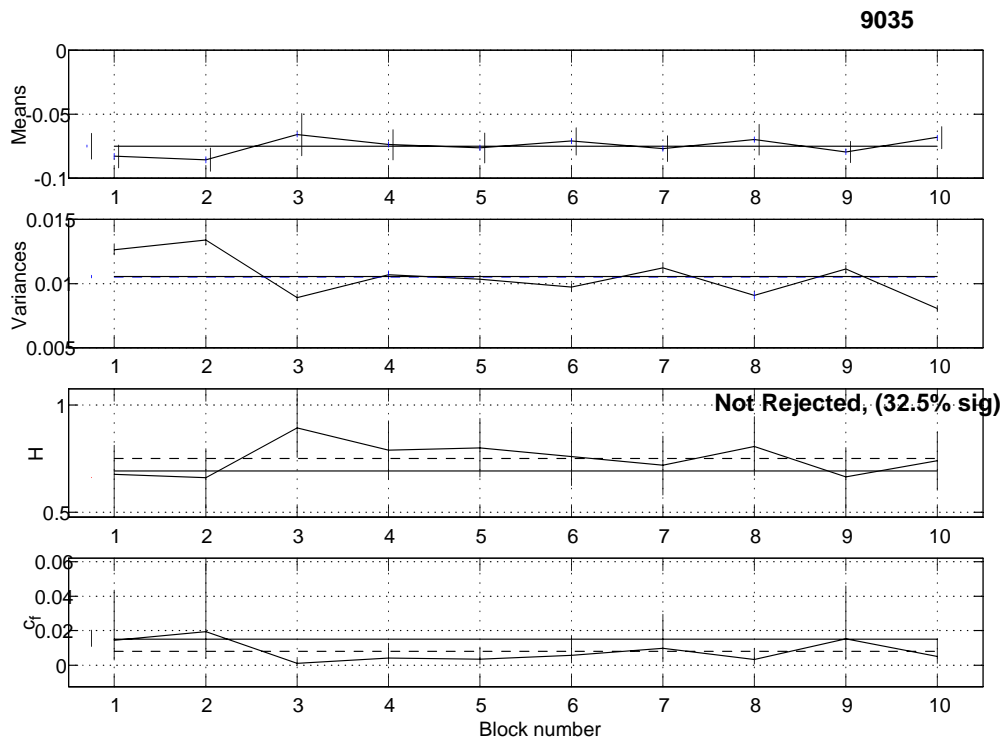


Figure 8: From top to bottom: means, variances, Hurst exponents and c_f 's evaluated over each block for signal 9035. On means and variances diagram horizontal line gives the overall value for the entire series. On H and c_f diagram solid horizontal line indicates the overall value and the dashed line gives the average value.

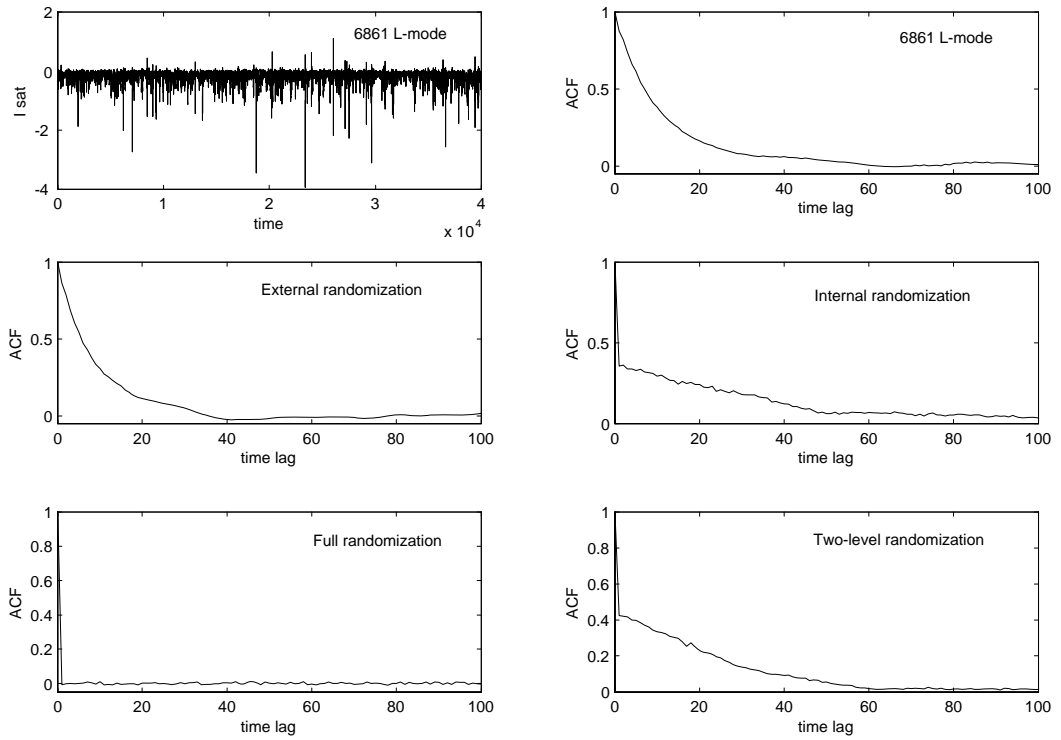


Figure 9: Top left: signal 6861; top right: autocorrelation function. The other diagrams are obtained by performing internal, external, total and two-level randomization as indicated.

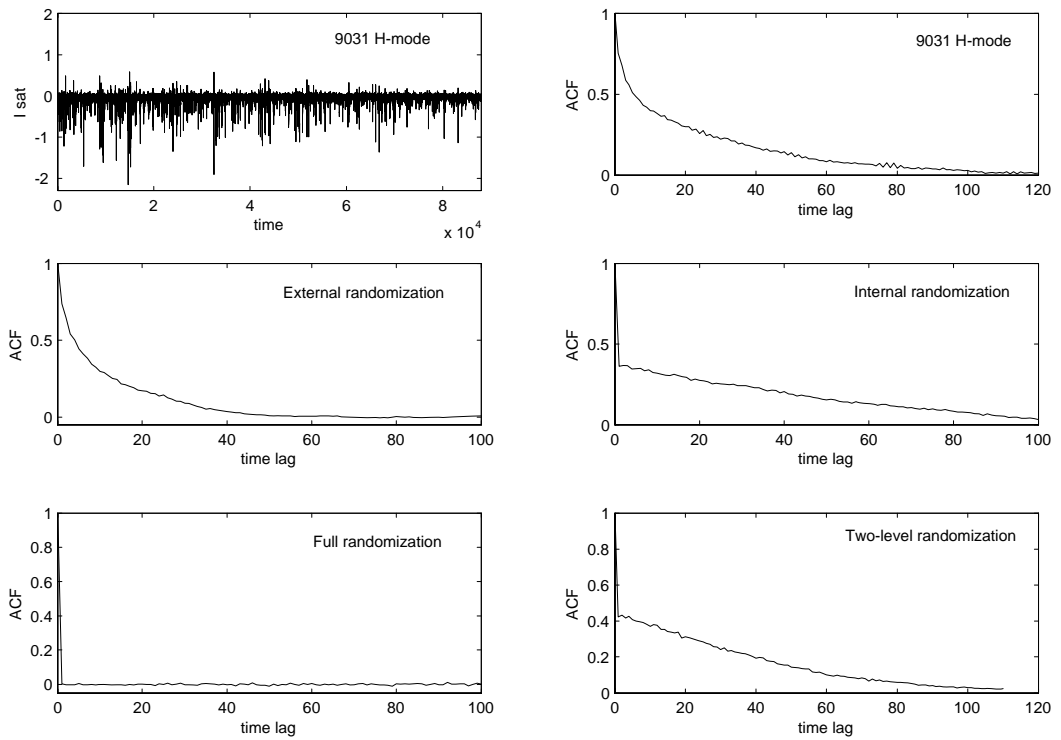


Figure 10: Top left: signal 9031; top right: autocorrelation function. The other diagrams are obtained by performing internal, external, total and two-level randomization as indicated.

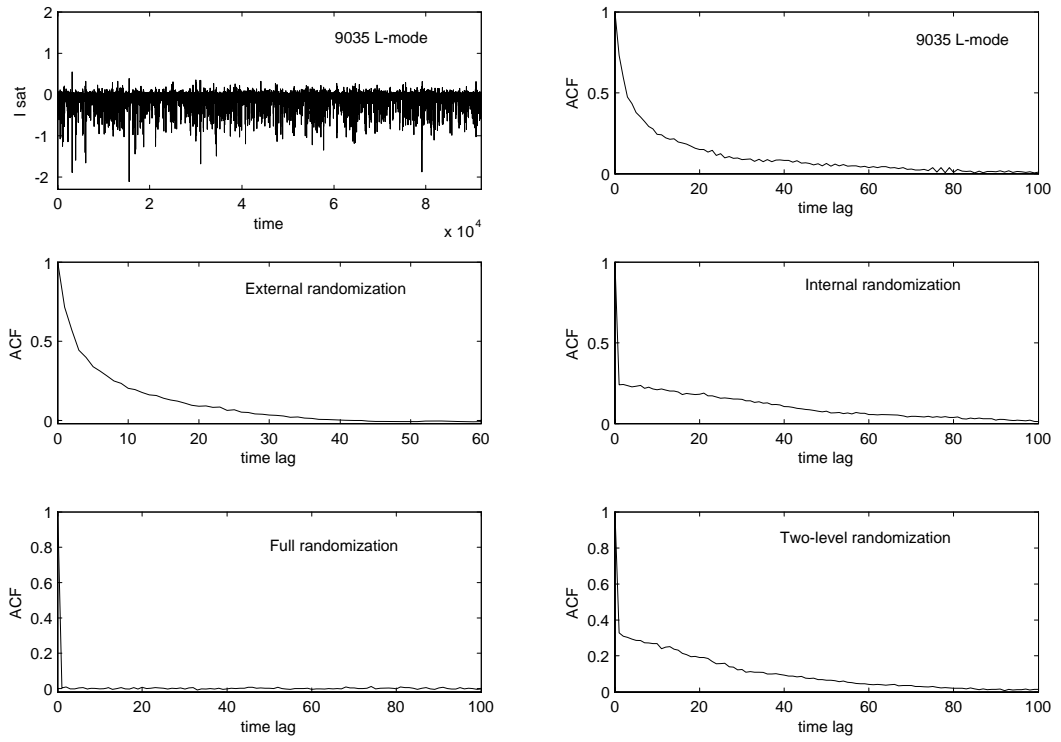


Figure 11: Top left: signal 9035; top right: autocorrelation function. The other diagrams are obtained by performing internal, external, total and two-level randomization as indicated.

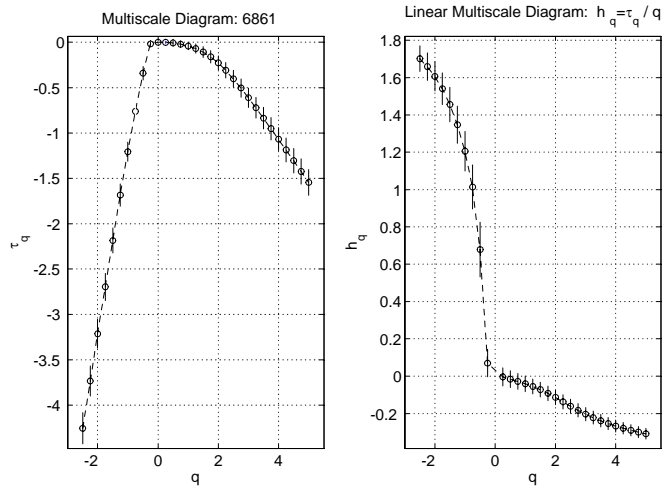


Figure 12: Multiscale and Linear multiscale (LM) diagrams for the 6861 L-mode regime. Lack of the flat region in the LM diagram indicates that the process is not globally self-similar.

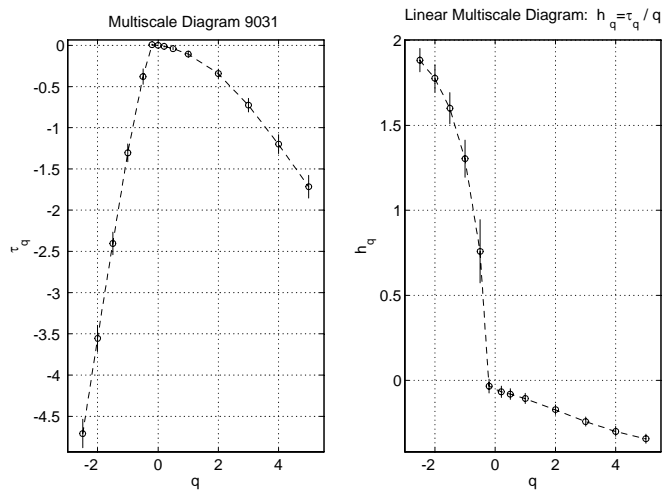


Figure 13: Multiscale and Linear multiscale (LM) diagrams for the 9031 H-mode regime. Lack of the flat region in the LM diagrams indicates that the process is not globally self-similar.

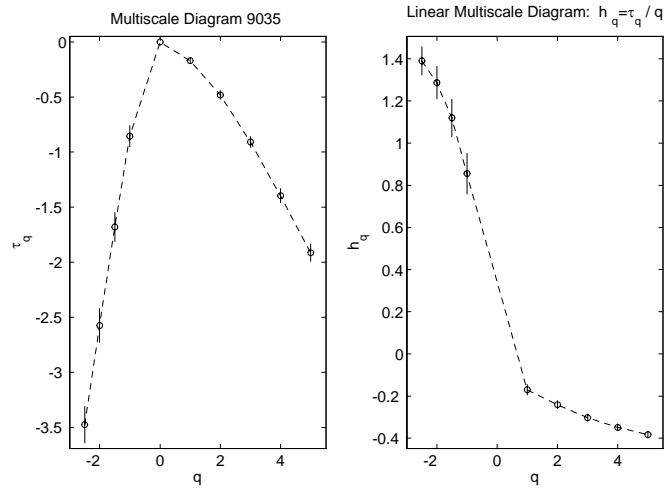


Figure 14: Multiscale and Linear multiscale (LM) diagrams for the 9035 L-mode regime. Lack of the flat region in the LM diagram indicates that the process is not globally self-similar.

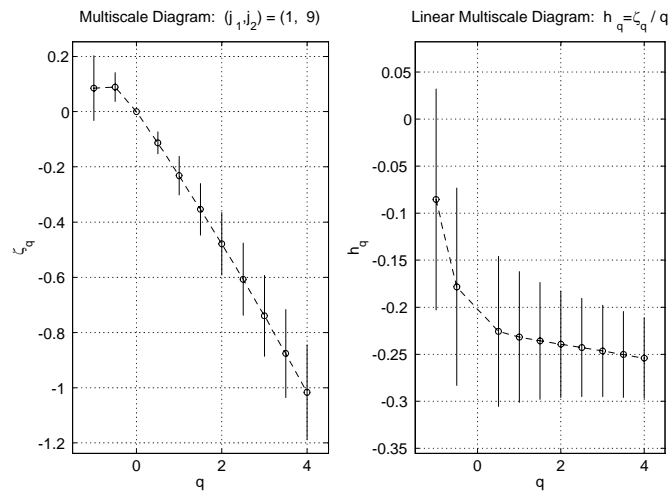


Figure 15: Multiscale and Linear multiscale (LM) diagrams for the fractional Gaussian noise. An almost flat region in the LM diagram for positive q indicates that the process is self-similar (a mono-fractal process).

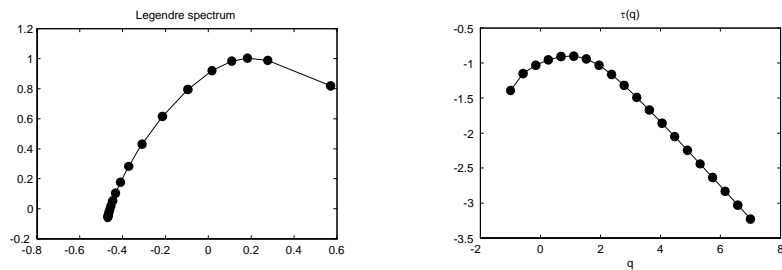


Figure 16: Multifractal spectrum (left) and $\tau(q)$ vs. q diagram (right) for the 6861 signal, obtained using the wavelet transform method.

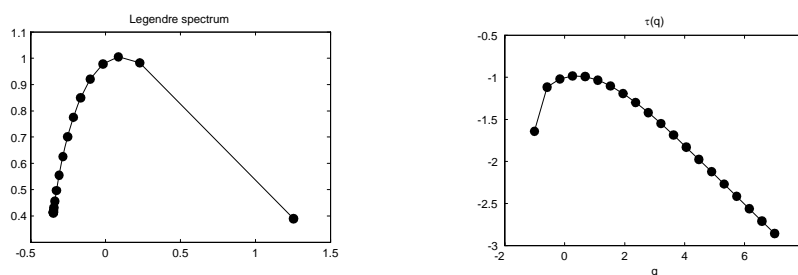


Figure 17: Multifractal spectrum (left) and $\tau(q)$ vs. q diagram (right) for the 9031 signal, obtained using the wavelet transform method.

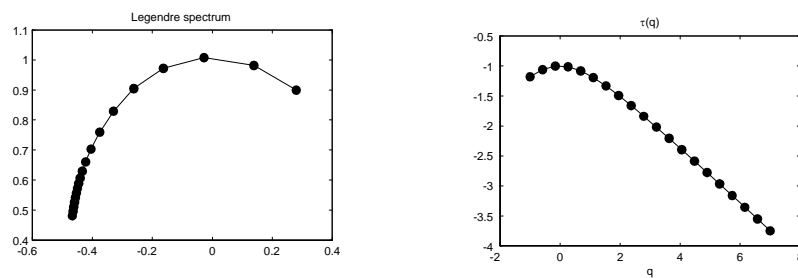


Figure 18: Multifractal spectrum (left) and $\tau(q)$ vs. q diagram (right) for the 9035 signal, obtained using the wavelet transform method.

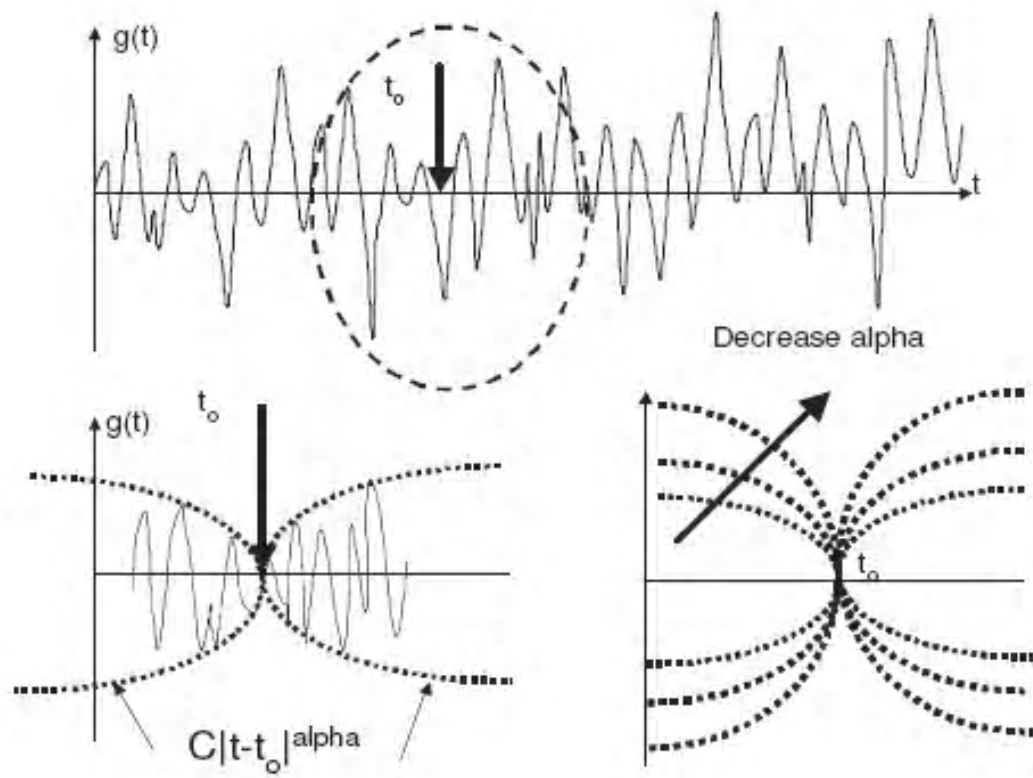


Figure 19: Geometric interpretation of local scaling exponent. Distribution of scaling exponents evaluated for the complete time series represents the multifractal spectrum.

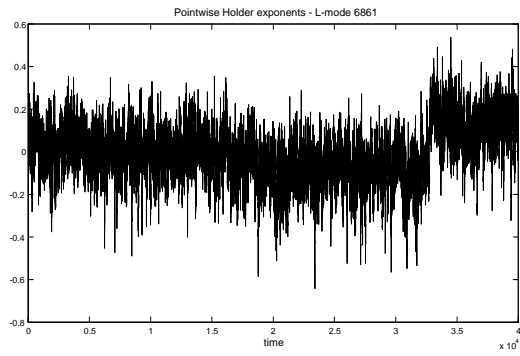


Figure 20: Pointwise Hölder exponents for the 6861 L-mode

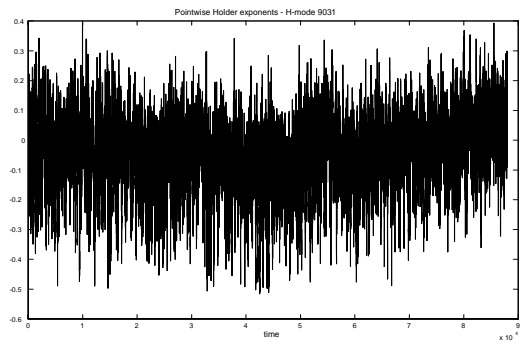


Figure 21: Pointwise Hölder exponents for the 9031 H-mode

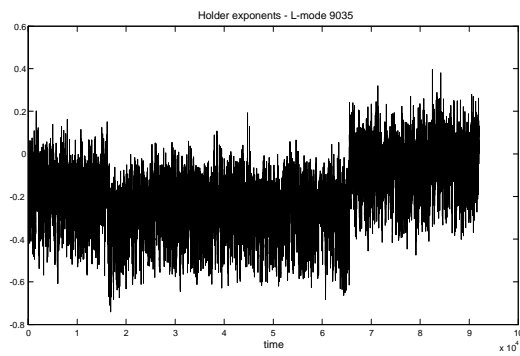


Figure 22: Pointwise Hölder exponents for the 9035 L-mode

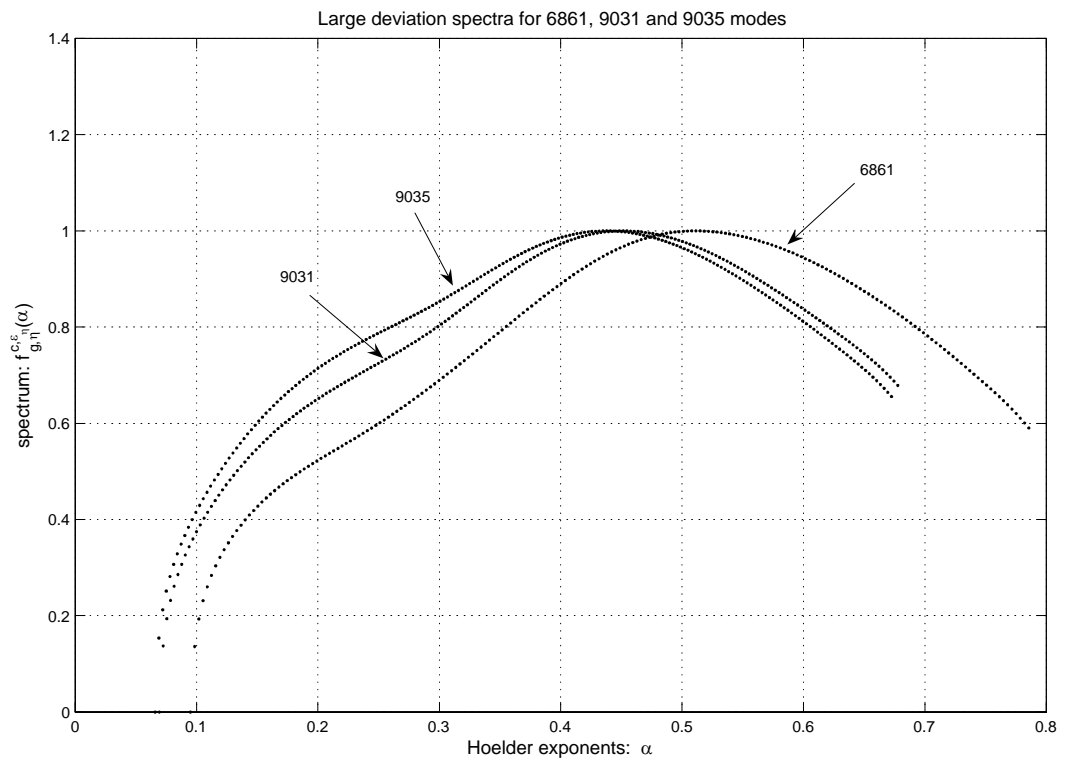


Figure 23: Large deviation spectra for the L-modes 6861 and 9035 and an H-mode 9031.

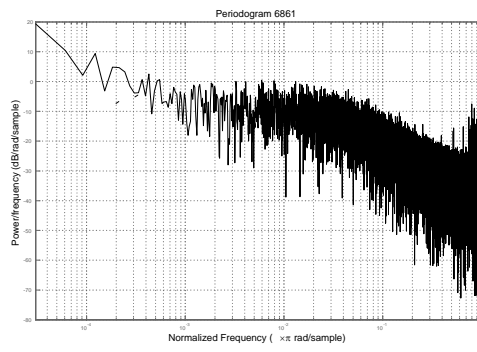


Figure 24: Periodogram of the L-mode 6861 signal.

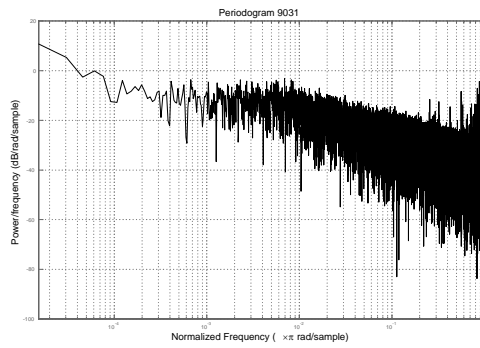


Figure 25: Periodogram of the H-mode 9031 signal.

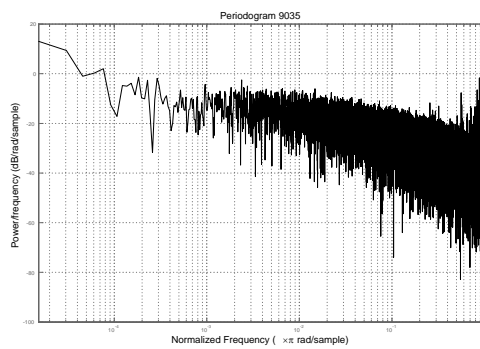


Figure 26: Periodogram of the L-mode 9035 signal.